Showcasing research from Prof. Ko's laboratory, Seoul National University, Korea and Prof. Chen's laboratory, Massachusetts Institute of Technology, Cambridge, United States.

Towards decarbonization in transportation: scalable transparent radiative cooling for enhanced vehicle energy efficiency

Vehicles exposed to sunlight heat up rapidly, increasing HVAC energy use. Transparent radiative cooling (TRC) offers passive heat mitigation, but prior approaches lacked optical clarity, durability, and real-world validation. We developed a scalable transparent radiative cooling (STRC) film for vehicle windows with >70% visible transmittance, strong mid-infrared emission, and high solar reflectance. Full-scale tests across regions and vehicle types showed up to 6.1 °C cabin temperature reduction and over 20% energy savings, with minimal winter penalty. U.S. fleet modelling projects 25.4 Mt annual CO_2 reduction.

Image reproduced by permission of Seung Hwan Ko from *Energy Environ. Sci.*, 2026, **19**, 1517.

As featured in:

See Seung Hwan Ko, Gang Chen *et al.*, *Energy Environ. Sci.*, 2026, **19**, 1517.

ROYAL SOCIETY OF CHEMISTRY

rsc.li/ees

Registered charity number: 207890

Energy & Environmental Science

ROYAL SOCIETY OF CHEMISTRY

PAPER

View Article Online
View Journal | View Issue

Cite this: *Energy Environ. Sci.*, 2026, **19**, 1517

Towards decarbonization in transportation: scalable transparent radiative cooling for enhanced vehicle energy efficiency

Min Jae Lee,[ab] Xuanjie Wang,[ci] Tae Han Kim,[d] Rohith Mittapally,[c] Won Sik Kim,[e] Young Ko,[c] Bong Jae Lee,[f] Jae Hyun Song,[d] Hyung Jun Lee,[d] Doo Nam Moon,[g] Seung Hwan Ko *[ah] and Gang Chen *[c]

Received 3rd November 2025,
Accepted 6th January 2026

DOI: 10.1039/d5ee06609c

rsc.li/ees

Vehicles exposed to sunlight experience rapid heating due to low thermal mass and confined space, leading to excessive HVAC energy consumption. Transparent radiative cooling (TRC) provides a passive pathway for heat mitigation, but existing TRC technologies face limitations in optical clarity, durability, and real-world validation. Here, we present a scalable transparent radiative cooling (STRC) film for vehicle windows, achieving >70% visible transmittance, strong mid-infrared emittance, and high solar reflectance. Full-scale field tests across various regions and vehicle types show substantial cabin temperature reductions of up to 6.1 °C and energy savings exceeding 20%, with a minimal winter heating penalty of 0.3%. Seasonal analysis and U.S. fleet-scale modeling further project an annual CO_2 reduction of 25.4 megatons—equivalent to removing 5 million cars from the road. STRC thus provides a practical, durable, and zero-energy cooling solution for sustainable and decarbonized transportation.

Broader context

Transparent radiative cooling (TRC) is a promising zero-energy strategy for passive cooling, but most prior studies have focused on buildings with large thermal mass. Vehicles, in contrast, heat rapidly under solar exposure due to low thermal mass and confined cabin volume, leading to severe overheating and increased cooling demand. Applying TRC to vehicles has remained challenging due to constraints in high optical transparency, scalable manufacturing, long-term durability, and full-scale real-world validation. Here, we develop a scalable transparent radiative cooling (STRC) film for vehicle windows. STRC combines high solar reflectance, strong mid-infrared emission, and visible transmittance that meets regulatory requirements, while maintaining optical and environmental durability under automotive-relevant conditions. We validate STRC through full-scale field tests across continents, seasons, vehicle types, and glass configurations, including full coverage and selective window applications. STRC consistently reduces cabin temperature and cooling energy demand under both parked and driving conditions. Seasonal analyses show that summer benefits outweigh minimal winter penalties, enabling annual net energy savings. A nationwide model further projects substantial CO_2 reduction with large-scale adoption, establishing STRC as a practical solution for decarbonized vehicle thermal management.

[a] *Department of Mechanical Engineering, Seoul National University, Seoul, Korea. E-mail: maxko@snu.ac.kr*
[b] *Energy Device Research Team, Hyundai Motor Company, Uiwang-si, Gyeonggi-do, Korea*
[c] *Department of Mechanical Engineering, Massachusetts Institute of Technology, Cambridge, Massachusetts, USA. E-mail: gchen2@mit.edu*
[d] *Thermal Energy Test Team 2, Hyundai Motor Company, Hwaseong-si, Gyeonggi-do, Korea*
[e] *Vehicle Thermos-Fluid CAE Team, Hyundai Motor Company, Hwaseong-si, Gyeonggi-do, Korea*
[f] *Department of Mechanical Engineering, Korea Advanced Institute of Science and Technology, Daejeon, Korea*
[g] *Carbon Neutrality Technology Innovation Team, Hyundai Motor Company, Uiwang-si, Gyeonggi-do, Korea*
[h] *Institute of Advanced Machinery and Design (SNU-IAMD)/Institute of Engineering Research, Seoul National University, Seoul, Korea*
[i] *Mechanical Engineering and Mechanics, Lehigh University, Bethlehem, Pennsylvania, USA*

Introduction

To reduce the energy demand of automotive heating, ventilating, and air conditioning (HVAC) systems without using additional external power, it is essential to minimize the thermal energy entering the cabin, particularly through windows, which account for over 40% of the total incoming thermal load.[1] Achieving this under real-world automotive conditions, where the interior temperature fluctuates rapidly,[2] poses a significant challenge due to the inherently conflicting requirements of high visible transparency and effective thermal rejection for windows. Conventional passive strategies such as low-emissivity (Low-E) coatings[3–5] mainly focus on reducing the inward transmission of solar radiation. However, their inability

to release internal mid-infrared (MIR) radiation trapped inside the vehicle[6] leads to greenhouse effects. Radiative cooling technologies address this challenge by combining solar reflectance with MIR thermal emission *via* the atmospheric window (8–13 μm) to outer space at 3 K,[7–23] offering energy-saving potential for daytime applications. Lv *et al.* demonstrated that the use of a radiative cooling cover on parked vehicles can significantly reduce the cabin temperature.[24]

Recently, transparent radiative cooling (TRC) has emerged as a promising approach for potential application in building windows[25–31] to simultaneously reflect sunlight and emit thermal radiation while preserving visible transparency. Most TRC technologies for space cooling have primarily focused on the optical properties of the top layer, namely its selective emittance (SE):[32] maximizing the emittance in the atmospheric transparent window to allow radiative cooling from the surface to the outer space while minimizing absorptance in the other infrared window to cut down the radiative heating of the surface by the surrounding. This strategy is effective when the surface remains below the ambient temperature, making it suitable for buildings or systems with relatively low and stable interior temperatures. However, unlike buildings with large thermal mass and slow temperature variation, vehicles exposed to direct sunlight experience rapid heating, and their interior temperature often exceeds the ambient temperature.[2] In such above-ambient conditions, SE—which maximizes thermal radiation only within the atmospheric transparency window while suppressing emission elsewhere—is less effective. Instead, broadband emitters (BEs) become advantageous, as they can radiate heat over a wider spectral range, including both the atmospheric window and non-window regions, enabling efficient heat dissipation to the sky and surrounding environment (Fig. S1). This rapid heat accumulation contributes significantly to thermal discomfort for occupants.[33,34] Despite the promise of TRC, previous developments have been limited to small-scale and laboratory demonstrations.[25,26,28,29,35,36] These advances are not sufficient for practical vehicle deployment due to limited visible transparency or insufficient heat reduction. Realizing a solution for automotive applications with high visible transparency, strong heat rejection, and scalable manufacturing have not been validated under real-world automotive environments.

In this work, we present a scalable transparent passive radiative cooling (STRC) film strategy designed for real-world vehicle applications, demonstrating substantial energy-saving performance under practical driving and parking conditions. This approach utilizes the full solar and thermal radiation spectrum by integrating high visible transmittance with visibility regulations, near-infrared (NIR) reflection, strong MIR absorption for cabin facing surfaces and large MIR emission for outer surfaces into a multilayered design. In particular, we use broadband MIR emitters since the cabin temperature is more often above the ambient temperature, enabling the cabin heat to be radiated both to outer space through the atmospheric transparency window and to the surroundings in the rest of the spectrum. Although the advantage of such BEs is recognized in some literature,[28] we demonstrate *via* experiments the advantage of such BEs over SE. The proposed STRC film is fabricated using scalable roll-to-roll manufacturing processes, ensuring practical viability for large-scale deployment while maintaining strong environmental durability. Based on STRC design, we report on the successful implementation of STRC in real vehicles. Through extensive full-scale field evaluations across different continents, vehicle types, and glass configurations, we demonstrate STRC's consistent performance in both static (parking) and dynamic (driving) scenarios, over wide seasons, especially in summer. To the best of our knowledge, this study represents the first systematic evaluation of STRC performance in full-scale vehicle settings. STRC achieved a cabin air temperature reduction of 6.1 °C and cooling energy savings of 20% during summer, which far outweighs minimal heating differences of 0.3% in winter, compared to uncoated control vehicles, resulting in meaningful net annual reductions in HVAC loads and associated carbon emissions. Partial deployment of STRC on the sunroof or front window still yielded substantial cooling and energy efficiency gains. Scaled across the U.S. vehicle fleet, these improvements could reduce annual CO_2 emissions by an estimated 25.4 megatons, equivalent to removing 5 million cars from the road. Comfort modeling reveals that STRC accelerates the time to achieve thermal comfort by 17 minutes. Our results demonstrate a promising pathway for addressing the critical challenge of vehicle cabin cooling under real-world conditions. By enhancing passenger comfort and offering a passive, high-efficiency solution, the proposed STRC can significantly reduce both energy consumption and transportation-related carbon emissions.

Results and discussion

Design and vehicle test overview

The STRC film is optimally designed to reduce vehicle thermal loads through a spectrally selective multilayer structure that modulates heat transfer across the visible, NIR, and MIR spectra (for more details, see experimental procedures). The STRC film consists of four functional layers (Fig. 1A), each engineered to perform distinct optical roles across specific wavelength ranges. The bottom layer broadly absorbs thermal radiation from the vehicle interior, while the top layer efficiently emits heat to outer space and the ambient environment in the MIR region. Sandwiching between them are two intermediate layers that reflect NIR radiation, specifically targeting the solar A region (780 to 1400 nm) and B band region (1400 to 2500 nm). This BE/broad absorption (BA) configuration is critical for enabling efficient radiative heat dissipation when the vehicle cabin temperature approaches or exceeds the ambient environment[28]—a scenario where the traditional Low-E film is largely ineffective. The BA component maximizes thermal absorption from the interior-facing side, while the BE layer ensures that heat is externally emitted to the ambient environment. This thermal regulation strategy allows the STRC film to act as a net emitter of heat under real-world automotive conditions.

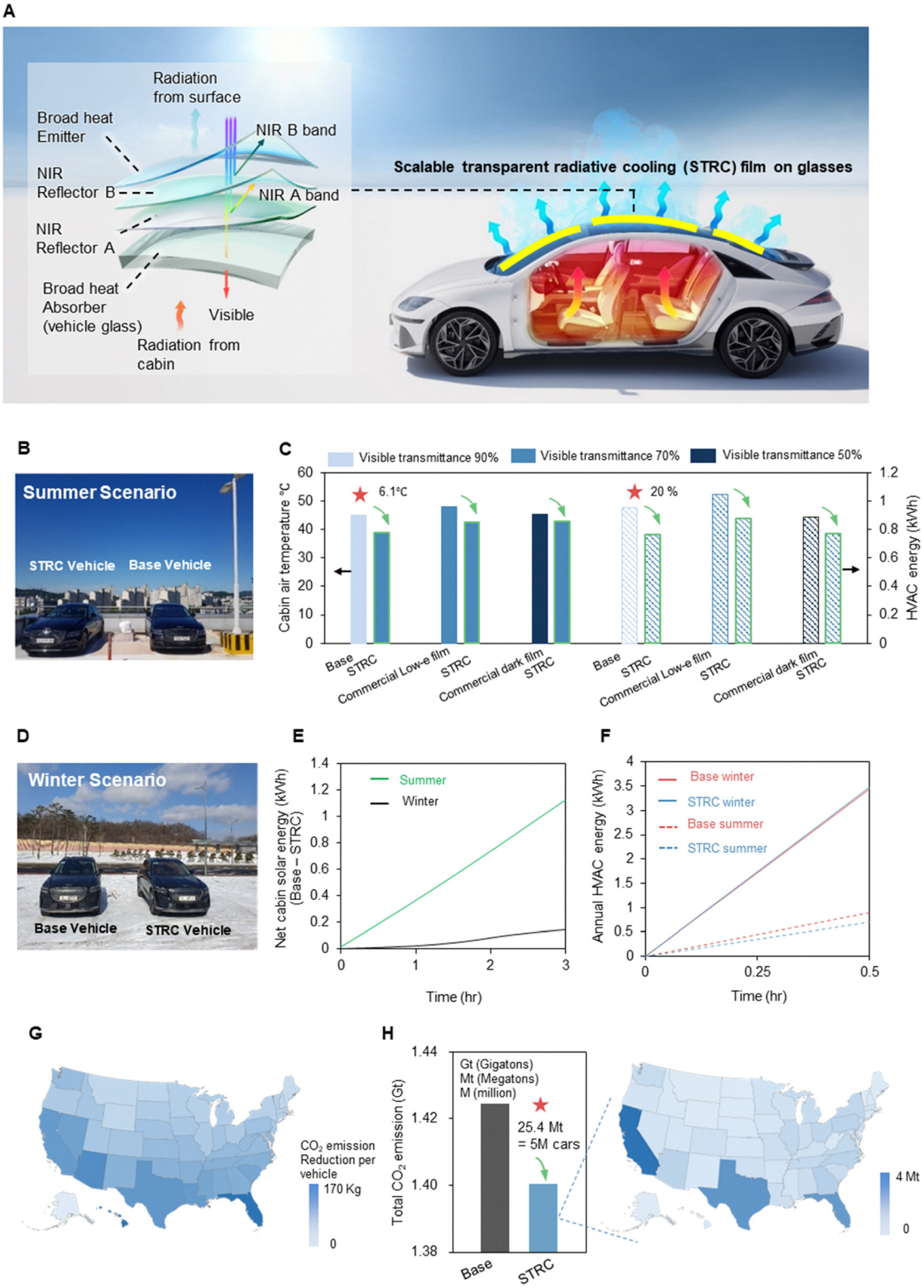

Fig. 1 Design and vehicle test overview. (A) Schematic of the STRC on a vehicle glasses, showing four-layered structure designed to manage radiation in the visible, near-infrared (NIR), and mid-infrared (MIR) bands. (B) Photograph of vehicle test in summer scenario. (C) Measured vehicle cabin air temperature and HVAC energy consumption compared with commercial films in difference transmittance. (D) Photograph of vehicle test in winter scenario. (E) Simulated vehicle net cabin solar energy (Base – STRC) in summer and winter. (F) Measured vehicle HVAC energy in summer and winter comparison with base vehicle. (G) Predicted US CO_2 emission reduction in kilogram (Kg) of STRC vehicle extended to all US states based on local climate zones. (H) Calculated US annual total CO_2 vehicle emissions in gigatons. Saving total 25.4 Megatons is equivalent to removing 5 million cars from the road.

To validate this design, a sequence of field experiments was conducted under both summer and winter conditions using real vehicles outfitted with STRC films on all glass surfaces. In the summer scenario (Fig. 1B), parked vehicles under direct sunlight showed a 6.1 °C reduction in cabin air temperature and a 20% reduction in HVAC energy consumption compared to baseline vehicles (Fig. 1C). Compared to commercial Low-E films with a visible transmittance of 70%, STRC-equipped vehicles exhibited a 5.16 °C reduction in cabin temperature and a 16.1% reduction in HVAC energy usage.

Compared to a commercial dark-tinted film with 50% visible transmittance, STRC still delivered a 2.7 °C reduction in cabin temperature and a 12.8% reduction in energy consumption, primarily due to its superior NIR reflectance and MIR emittance (Fig. S4). In the winter scenario (Fig. 1D), HVAC energy consumption was monitored to determine the net seasonal energy impact. A net solar load inside the cabin between the base and STRC vehicles was evaluated by vehicle simulation under both summer and winter during parking conditions (Fig. 1E). The total measured HVAC energy usage across an annual cycle is lower for STRC vehicles compared to conventional vehicles (Fig. 1F). This outcome is attributed to the seasonal asymmetry: while the passive cooling benefits in summer are substantial due to higher irradiance and longer solar exposure, the winter heating penalty is minimal owing to less solar energy in the average of winter so that the gain of NIR radiation is small even with a fully visibly transparent window. As a result, STRC implementation delivers significant net annual energy savings.

Extending beyond individual vehicle performance, the system-wide benefits of STRC adoption were modeled at a national scale. Using climate-specific HVAC usage profiles and regional driving data, the projected annual reduction in CO_2 emissions was calculated when the STRC vehicle was deployed in the United States (U.S) (Fig. 1G). The analysis with entire passenger vehicles in the U.S revealed substantial annual CO_2 emission reductions of 25.4 megatons (Fig. 1H) equivalent to removing over five million gasoline cars based on an average of 4.6 tons CO_2 per vehicle per year.[37]

Photonic design, optical performance, and durability characteristics of the STRC film

The combined performance of all the layers is demonstrably linked to the strategic selection of the emitter and absorber in the MIR range. The power-density calculations performed for both day (Fig. 2A) and night (Fig. S5) conditions demonstrated superior heat dissipation for BE/BA compared to SE/selective absorption (SA).

The figure clearly shows the distinctly two different regimes for STRC. When the cabin temperature is above the ambient temperature, the BE/BA combination in MIR works best to reduce the cabin temperature. To validate the thermal performance of different MIR optical combinations, a series of outdoor field measurements were performed in Massachusetts, U.S using an insulated chamber (Fig. 2B). Comparative averaged cabin air temperature data (Fig. 2C) demonstrated that STRC achieved significantly greater cooling, lowering interior temperatures by 11.9 °C, 5.1 °C, and 1.7 °C compared to standard window glass, Low-E/BA, and SE/BA configurations, respectively. Detailed experimental setups and results are presented in Fig. S6–S9. Complementary simulation results also verified that the BE/BA configuration yielded the lowest internal temperatures across different MIR spectral combinations (Fig. S10). Further comparison with commercial Low-E and oxide/metal/oxide (O/M/O) films[38,39]—based on the measured optical properties—reinforced STRC's superior thermal performance (Fig. S11 and S12).

Scalability was achieved through the development of a roll-to-roll manufacturing process, enabling continuous production of the STRC film up to 1600 mm in width (Fig. 2D), sufficient to cover all vehicle windows including panoramic sunroofs. When laminated onto 2.1 mm thick automotive glass, the STRC film maintained an average visible light transmittance of 74.7% across the 400–780 nm range, thus meeting ISO 3537 visibility standards required for global front window approval (Fig. 2E). Additionally, the STRC film demonstrated 76.8% NIR reflectance and 80% MIR emittance of the outer surface, with an MIR absorption of 89% for the bottom cabin facing surface (Fig. 2E; see also Fig. S13). Optical durability was validated through long-term UV exposure testing. After two years of accelerated aging, the film's total and diffuse transmittance in the visible range showed negligible degradation (Fig. 2F), maintaining optical properties. Mechanical robustness was tested with tensile stress characteristics remaining stable after 500 thermal cycles between −20 °C and 80 °C (Fig. 2G). Moreover, differential scanning calorimetry (DSC) analysis (Fig. 2H) confirmed that the STRC film maintains chemical stability throughout the tested temperature range of –40 °C to 90 °C exceeding the extreme interior temperatures typically observed in closed vehicles during both summer and winter. Additional assessments of hydrophobicity, Vickers hardness, and surface roughness (Fig. S14) further demonstrated the film's mechanical robustness and environmental durability, underscoring the suitability for real-world vehicle applications.

Real-world thermal performance of STRC in vehicles

To evaluate the passive cooling performance of STRC in vehicles, a comprehensive series of field tests were conducted on parked vehicles during summer conditions across diverse geographic locations, vehicle types, and film deployment strategies (Fig. 3). Each vehicle was equipped with 23 thermocouples to measure cabin air and glass surface temperatures under identical ambient conditions before STRC application (Fig. S15). The purpose of this test was to confirm that both vehicles exhibited similar baseline thermal responses and that all thermocouples and data acquisition systems were functioning correctly. This pre-validation step ensured that any temperature differences observed during subsequent STRC evaluation could be confidently attributed to the STRC film itself rather than to sensor errors, instrumentation drift, or vehicle-to-vehicle variability.

In Case 1, electric sedans and sport utility vehicles (SUVs) in Namyang, Korea, were equipped with the STRC film on all

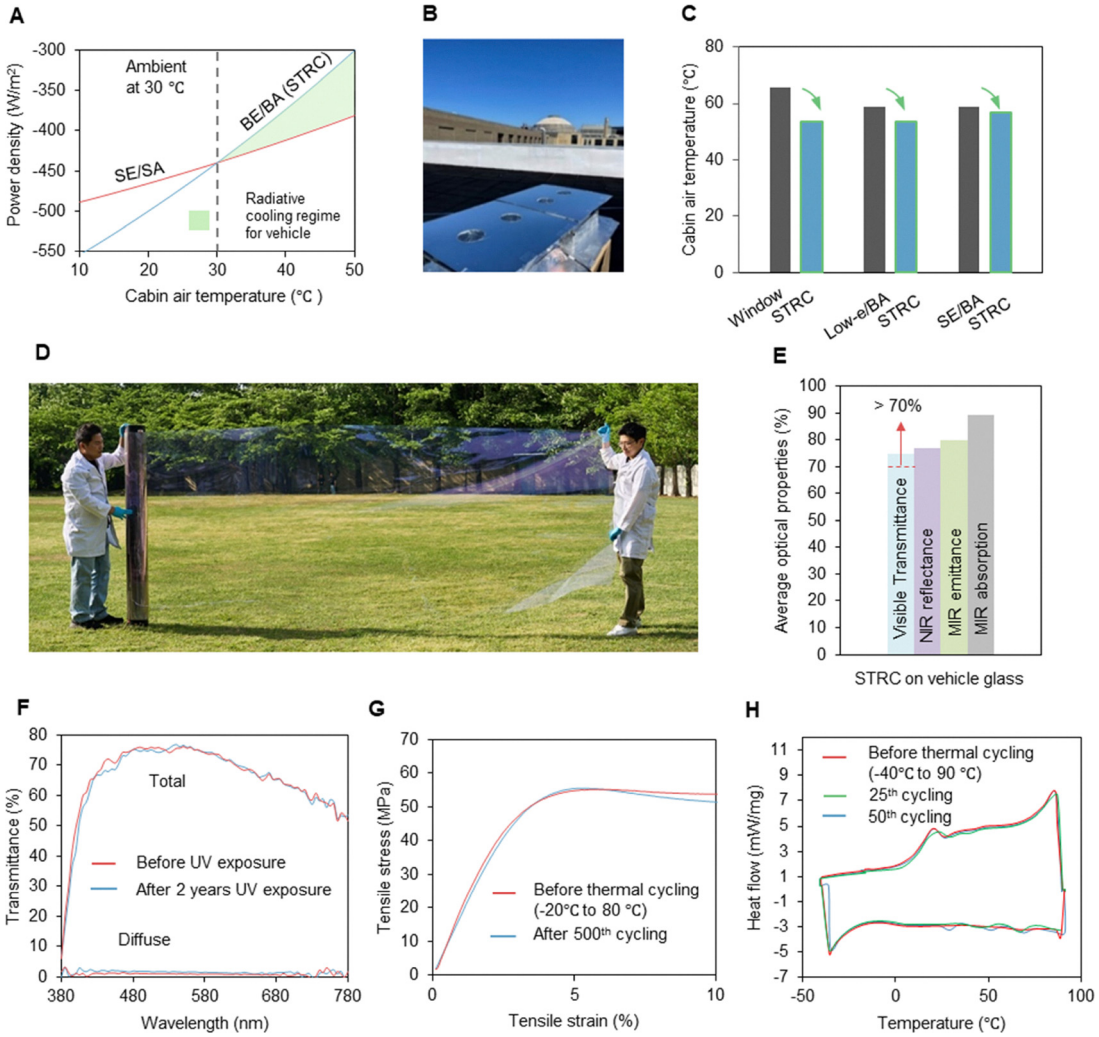

Fig. 2 Features of the STRC film. (A) Calculated net cooling power density of the STRC film as a function of cabin temperature at an ambient temperature of 30 °C, using ideal optical properties for broadband emission/absorption (BE/BA) and selective emission/absorption (SE/SA) designs. Negative values indicate heat gain, where the surface absorbs more energy than it emits. Under the tested conditions, the STRC film exhibits lower heat gain compared to the SE/SA configuration when cabin air temperature is above the ambient temperature. (B) Photograph of outdoor temperature measurement setup (C) Measured average cabin air temperature performance comparison with different optical combination between Low-e/BA, and SE/BA. (D) Photograph showing STRC film of the width 1600 mm (E) Measured average transmittance in the visible from 480 nm to 780 nm, reflectance in the NIR regions from 790 nm to 2500 nm, and emittance/absorbance in the MIR region from 4 to 18 μm. STRC on vehicle 2.1 mm glass has transmittance over 70% by ISO 3537 (F) Optical durability result in the visible range showing the total and diffuse of STRC film before and after 2 years UV exposure test. (G) Mechanical durability result in tensile stress before and after 500th cycling between −20 °C to 80 °C. (H) DSC of STRC film before and after 50th cycling between −40 °C to 90 °C.

exterior window surfaces, including the front, sides, rear, and sunroof glasses (Fig. 3A). The results (Fig. 3B) confirmed that STRC-equipped vehicles exhibited substantially lower cabin air temperatures—averaging a reduction of 3.0 °C in sedans and 2.3 °C in SUVs—after four hours of direct solar exposure. All exterior glass surfaces also showed reduced temperatures (Table S1), demonstrating the benefit of full-system STRC coverage. To examine partial implementation, Case 2 evaluated thermal performance when STRC was applied only to the front window. After two hours of solar exposure, the cabin air temperature was reduced by an average of 1.5 °C (Fig. 3C and D), and both the inner and outer surfaces of the front glass were cooler than in the baseline configuration (Fig. 3E). These results confirm that even localized applications of STRC can deliver meaningful passive cooling benefits. In Case 3, the experiment focused on the rooftop window, with STRC film applied exclusively to the sunroof. The test included various sunroof blind positions and compared the STRC-equipped sunroof (with the blind fully open) against a baseline sunroof (with the blind fully closed) (inset photo of Fig. 3F). Despite the disadvantageous setup, the STRC configuration yielded superior performance, lowering the interior cabin air temperature by an average of 1.3 °C across all conditions (Fig. 3F and G). Surface temperatures of the sunroof were also markedly reduced, reinforcing the importance of rooftop solar rejection (Fig. 3H). Regional validation was performed in California,

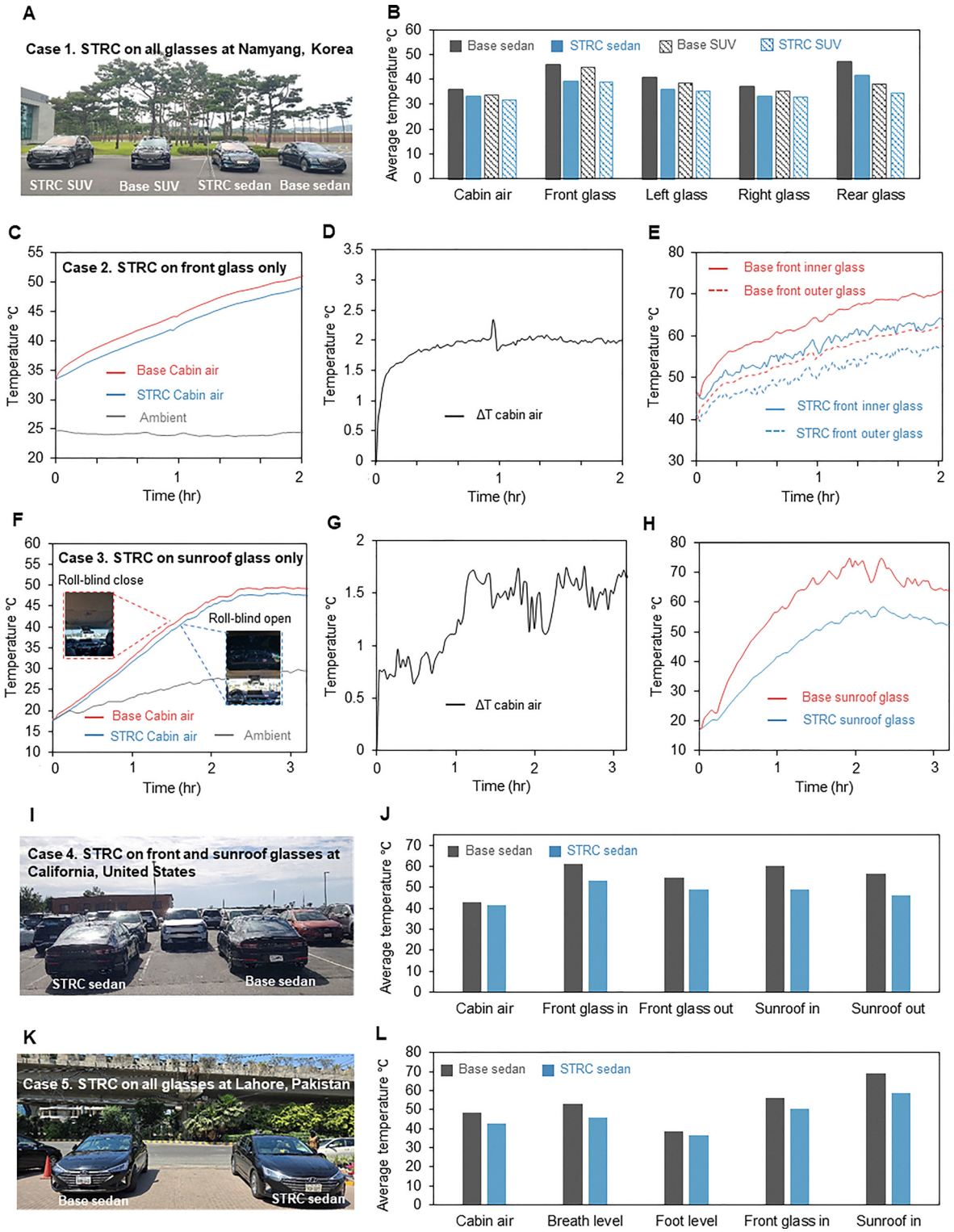

Fig. 3 Summer parking vehicle performance. (A) and (B) (Case 1) Photograph of four vehicles (two base sedan and STRC sedan, and two base SUV and STRC SUV) in Namyang, Korea. STRC film was applied to vehicles on all of glasses including front, side, rear (B) measured 4 hours average temperature of cabin air and inside surface temperature glasses (C)–(E) (Case 2) Measured cabin air temperature when STRC film applied to front glass only. (D) Cabin air temperature difference between Base and STRC (E) measured temperature on the inner and outer surface temperature of the front glasses (F)–(H) (Case 3) measured cabin air temperature when STRC film applied to sunroof glass only. (G) Cabin air temperature difference between Base and STRC (H) measured inside, and outside sunroof glasses surface temperature (I) and (J) (Case 4) photograph of two vehicles (two base sedan and STRC sedan) in California, U.S. STRC film was applied to vehicles on the front and sunroof glasses. (J) Measured 4 hours average temperature of cabin air and surface glasses temperature. (K) and (L) (Case 5) Photograph of two vehicles (two base sedan and STRC sedan) in Lahore, Pakistan. STRC film was applied to vehicles on all of windows including front, side, rear, sunroof (L) measured 4 hours average temperature of cabin air, breath level, foot level and inside surface temperature glasses.

U.S (Case 4), where the STRC film was applied to the front window and sunroof of sedans (Fig. 3I). Despite regional differences in the solar spectra and ambient conditions, the STRC-equipped vehicle consistently maintained lower cabin air and glass surface temperatures throughout the four-hour measurement period than in the baseline (Fig. 3J; see also Table S2). Lastly, STRC was tested under extreme summer conditions in Lahore, Pakistan, where a sedan was fully laminated with the STRC film on all exterior window surfaces (Fig. 3K). The measured data showed consistent reduction not only in cabin air temperature, but also at occupant-relevant levels such as the breathing height and foot level (Fig. 3L; see also Table S3). Collectively, the findings in Fig. 3 demonstrate that STRC consistently lowers internal cabin temperatures whether applied fully or partially across different vehicle types, film attached location, and global solar climates enabling scalable, passive cooling performance that can be tailored to retrofit applications.

Annual real-world energy performance of STRC in vehicles

To rigorously assess the real-world energy performance of STRC over different seasons and operating modes, a sequence of controlled vehicle experiments was conducted in parking and driving states. These experiments captured detailed thermal and HVAC performance data under both summer and winter conditions using STRC equipped vehicles. Case 6, involving STRC films applied on all glass surfaces, replicated summer parked vehicle conditions by exposing vehicles to 670 W m^{-2} solar irradiance at 23 °C ambient temperature for four hours (inset photo of Fig. 4A). After thermal soaking with the A/C off, the A/C system was activated. Compared to the baseline, the STRC-equipped vehicle exhibited 6.1 °C lower cabin air temperature and a 20% reduction in A/C energy consumption (Fig. 4A). Evaporator temperature and compressor RPM indicated faster thermal stabilization and reduced cycling demand (Fig. 4B), highlighting STRC's benefit in minimizing cooling loads after solar exposure. Case 7, also with the STRC film on all windows, evaluated winter parked vehicle performance under −5.2 °C ambient temperature and 400 W m^{-2} solar irradiance (inset photo of Fig. 4C). After 4-hour soaking, cabin heating was initiated. Although STRC vehicles showed slightly cooler averaged cabin temperatures of 2.3 °C, the heating energy consumption remained nearly identical to the baseline differing by only 0.4% (Fig. 4C). Floor-level temperature distributions and heating power data (Fig. 4D) confirmed that thermal comfort was preserved with less than 1% heating penalty. Case 8 assessed STRC performance during summer driving. The vehicle, equipped with the STRC film on the front and sunroof windows, was tested on a proving ground in California under 750 W m^{-2} solar irradiance and 27 °C ambient temperature while driving at approximately 55 km h^{-1} (Fig. 4E). The STRC vehicle consistently maintained a lower average cabin temperatures of 1.7 °C and a reduced A/C-related average fuel consumption of 7.0% throughout the drive (Fig. 4F), demonstrating its effectiveness under dynamic conditions involving airflow and solar variability. A full-vehicle three-dimensional thermal simulation was conducted under summer and winter conditions (Fig. S16). The calculated results also showed that the total annual HVAC energy consumption of STRC-equipped vehicles was lower than those of both Low-E and SE vehicles (Fig. S17). Together, these results confirm that STRC offers consistent thermal and energy-saving benefits across both static and dynamic use cases. Substantial summer cooling savings lead to net annual HVAC reductions, despite minimal winter heating penalties.

Thermal modeling and comfort simulations validating STRC performance

To systematically assess the energy-saving potential and thermal comfort benefits of the STRC film, a comprehensive vehicle energy balance model was developed. This model incorporated radiative, convective, and conductive heat transfer mechanisms under realistic solar loading, and was calibrated using experimental data.

In steady-state simulations (Fig. 5A), HVAC energy demand is plotted as a function of ambient temperature under a constant 1000 W m^{-2} solar load. The STRC-equipped vehicle consistently required less power than baseline and Low-E glass to maintain a cabin temperature of 22 °C. Transient simulations provided further insight. In summer (Fig. 5B), the STRC vehicle exhibited quicker reductions in cabin temperature and consumed significantly less energy to reach and maintain the comfort set point. In winter (Fig. 5C), the STRC cabin was slightly cooler, requiring marginally more heating energy (see the SI Note for details on the thermal model). However, these minor penalties were more than offset by substantial summer cooling savings, yielding a net annual HVAC reduction. Full-vehicle three dimensional (3D) simulations confirmed these trends: STRC delivered the coolest interiors in summer while matching the performance of SE and Low-E films in winter (Fig. 5D and E). Passenger comfort was also improved: the STRC vehicle reached face level comfort in summer 17 minutes faster than the baseline vehicle (Fig. 5F). Annual HVAC energy consumption under four hours parking and one hour HVAC usage driving conditions (Fig. 5G) confirmed that STRC minimized energy usage across all seasons compared to base, low-E and SE. The full-vehicle 3D simulation validation of cabin air temperature against measured data (Fig. 5H) showed excellent agreement of the minimum and maximum temperatures of 2 °C. These modeling results, consistent with experimental data, affirm that STRC is a robust, passive, and regulation-compliant solution for year-round vehicle climate control.

Conclusions

This study establishes STRC as a validated and scalable approach for passive thermal management in vehicles. Based on comprehensive field experiments, long-term environmental durability assessments, and physics-based simulations, we demonstrate that STRC consistently reduces cabin heat gain and HVAC energy consumption under real-world conditions—across parking and driving states, seasonal variations, and even

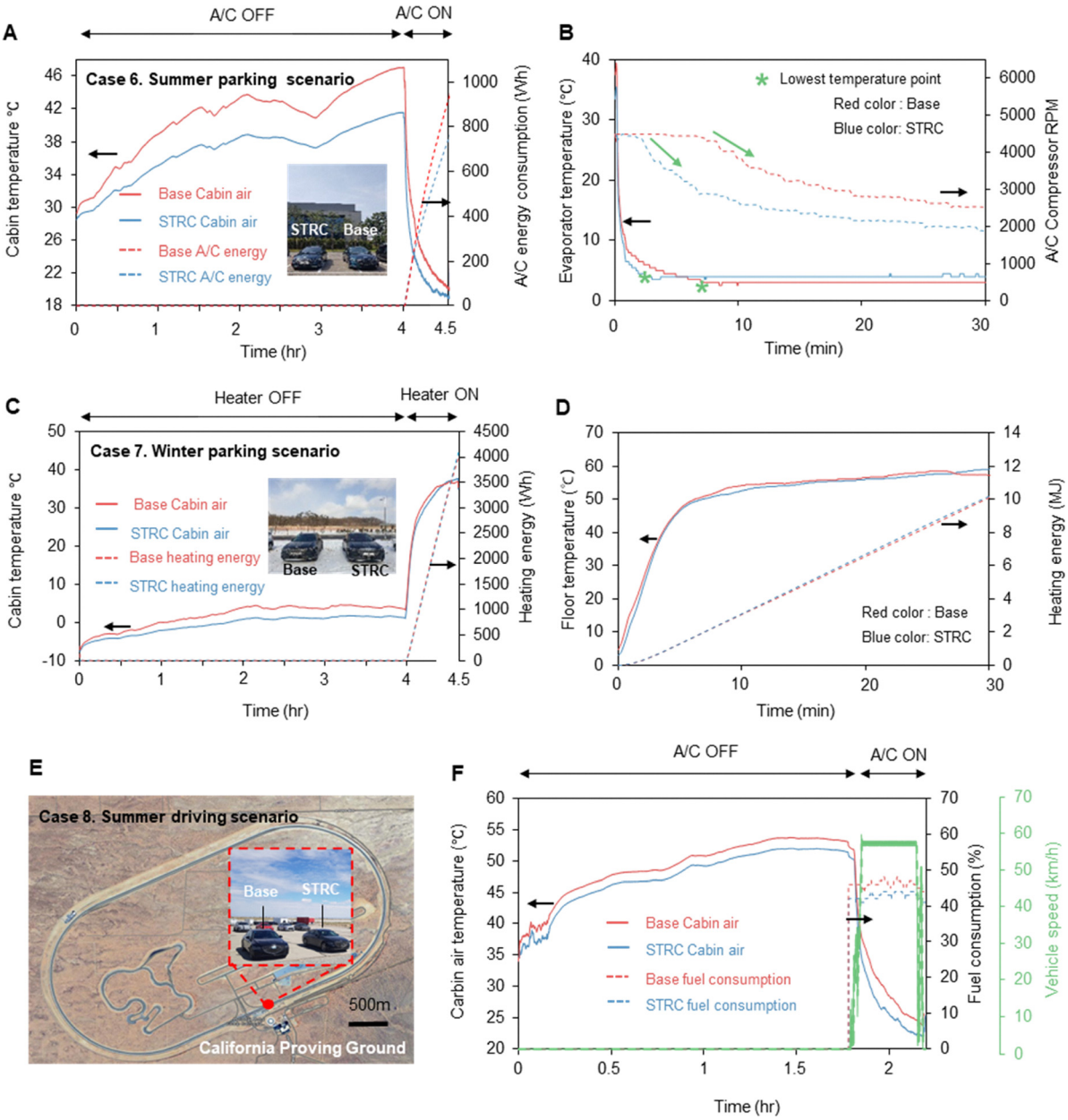

Fig. 4 Annual heating/cooling evaluation at parking and driving condition (A) and (B) (Case 6) measured cabin temperature (solid lines) and A/C energy consumption (dot lines). Turns A/C off for 4-hour thermal soaking and turns A/C on at parked state with 23 °C ambient and 670 W m^{-2}. (B) Measured evaporator temperature with A/C compressor RPM. Once the evaporator reaches its lowest temperature, A/C compressor RPM drops accordingly. (C) and (D) (Case 7) Measured cabin temperature (solid lines) and heating energy (dot lines) during winter. Turns heater off for 4 hours thermal soaking and turns heater on at parked state with −5.2 °C ambient and 400 W m^{-2}. (D) Measured floor temperature (solid lines) with heating energy (dot lines). (E) and (F) (Case 8) Photograph of two vehicles (base and STRC) in California Proving Ground parking lot before driving. (F) Measured cabin temperature (solid lines) and fuel consumption (dot lines). Turns A/C off for 4 hours thermal soaking and turns A/C on at driving 50 km h^{-1} (green solid line) with 27 °C ambient and 750 W m^{-2}.

when selectively applied to specific window surfaces. Moreover, STRC accelerates the attainment of passenger thermal comfort. Unlike conventional spectrally selective films, STRC employs a broadband photonic design that combines high visible transmittance, strong NIR reflectance, and efficient MIR emittance/absorption. This configuration enables radiative heat rejection when the vehicle cabin temperature exceeds the ambient temperature, offering passive cooling performance under thermal conditions where traditional technologies typically fail. The film is compatible with standard 2.1 mm vehicle glass and meets international transparency and safety regulations, facilitating practical deployment without compromising visibility. Its mechanical and optical durability under prolonged exposure to UV radiation, humidity, and thermal cycling further supports its viability for extended use in demanding environments. National level simulations indicate that the wide adoption of

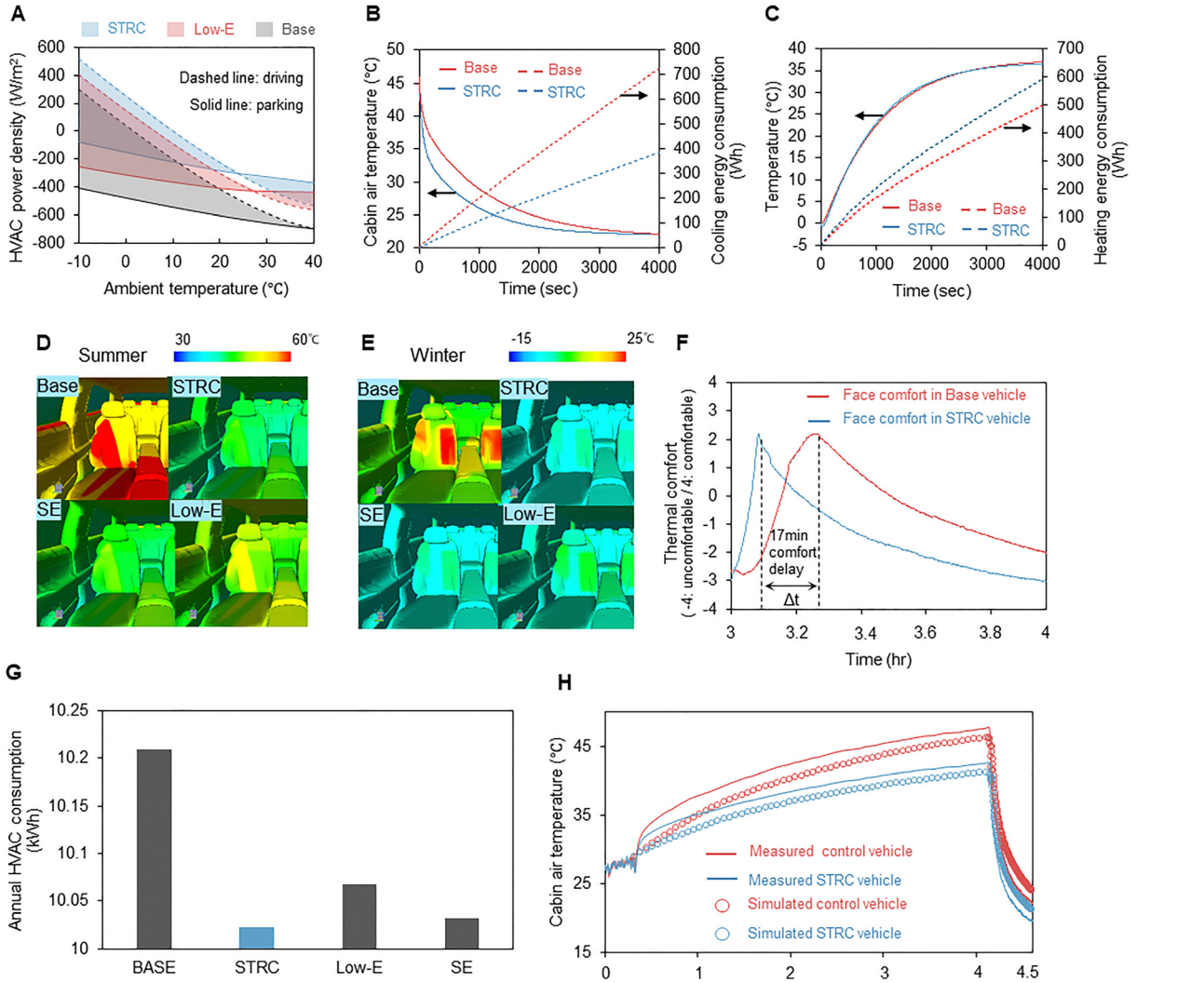

Fig. 5 Vehicle energy balance model and comfort simulation. (A) The HVAC energy consumption for parking (solid line) and driving (dotted line) modes to keep the cabin air at a comfort temperature of 22 °C with solar intensity 1000 W m^{-2} as a function of the ambient temperature is plotted for various cases. Note: Negative HVAC power density indicates cooling energy demand (AC operation), while positive values would represent heating demand (Heating). (B) Transient HVAC consumption (dotted line) and cabin air temperature (solid line) in the summer required to maintain the temperature at a comfort temperature of 22 °C. This model verified that STRC consumed less HVAC energy in the summer compared to the base. (C) Transient HVAC consumption (dotted line) and cabin air temperature (solid line) in the winter required to maintain the temperature at a comfort temperature of 60 °C. This model verified that STRC vehicle led to slightly cooler cabin temperatures, and heating energy consumption slightly increased, which means that cooling energy savings during summer far outweigh minimal heating differences in winter, resulting in meaningful net annual reductions in HVAC load (D and E) Full vehicle three-dimensional simulation of summer and winter scenario cabin air comparison with Base, STRC, SE, and Low-E (F) Time difference in reaching face-level thermal comfort after A/C activation. STRC vehicles reach 17 min faster than Base vehicle (G) Annual energy consumption comparison with Base, STRC, Low-E and SE (H) Cabin air value comparison with measured and simulated values.

STRC could lead to substantial reductions in vehicle energy use and associated carbon emissions. Although vehicle evaluations in this study were conducted only once per test condition due to the scale and complexity of the field tests, the consistent trends observed across different continents, vehicle types, glass configurations, and both static and dynamic over multiple seasons reinforce the overall reliability of the results. This technology requires no external energy input, operating passively and continuously regardless of the user behavior or external infrastructure.

Future developments may explore synergies with dynamic optical technologies, enabling responsive and multifunctional thermal control surfaces. While the current design offers significant advantages during summer, further research is needed to optimize performance during cold seasons.[40–43] Incorporating switchable optical properties that respond to temperature or electrical stimuli could enable not only reduced cooling loads in summer but also improved solar gain during winter by dynamically adjusting both their solar absorptivity and MIR radiation properties. Additionally, further investigation is needed into the impact of STRC on vehicle aesthetics and performance under a wide range of dynamic driving conditions. These efforts can pave the way for broader adoption of this promising technology as a scalable, energy-efficient solution for decarbonized transportation.

Experimental

STRC design guide

The STRC film consists of four layers that are optimally designed for enclosed cooling systems, such as vehicle cabins (Fig. S1). The top layer, composed of poly(methyl methacrylate) (PMMA), functions as a broad heat emitter. This layer is designed to release heat outwardly to both the atmosphere and outer space from the cabin in the MIR range (4–20 μm) and exhibits high transmittance in the visible and NIR spectra. Parked vehicles, where cabin temperatures often exceed ambient temperatures,[44] benefit significantly from the BE. Compared to the SE, as the cabin air temperature rises, the peak of the heat radiated from the cabin shifts toward shorter wavelengths and the BE enables more heat dissipation than the heat radiated from the sky.[45,46] Investigating the impact of varying the thickness of the top layer using a numerical model revealed that PMMA can have broadband emittance in the MIR spectrum (Fig. S2) that favors a reduction in the vehicle temperature for parked vehicles exposed to the sun. A thicker PMMA layer exhibits a higher BE cooling density (Fig. S2) and emittance when the vehicle temperature is higher than the ambient temperature. Considering the usability of the film, a PMMA thickness of 100 μm was chosen as the optimal thickness (Fig. S2).

The bottom layer, vehicle window, is composed of silicon dioxide (SiO_2) and serves as a BA in the MIR range (4–20 μm), similar to the broad spectrum of the top layer. The bottom layer is designed to exhibit high transmittance in the visible and NIR spectra, along with high absorbance in the MIR range. This design notably affects cooling in enclosures by absorbing more thermal radiation over a broad spectral range (4–20 μm) within the enclosure than in SA, regardless of the cabin air temperature. A substantial SiO_2 thickness compatible with existing vehicle windows ensures broad-spectrum absorbance across the MIR spectrum, effectively absorbing the heat generated by the enclosure (Fig. S2).

The two intermediate heat reflector layers require a high visible transmittance and high NIR reflectance because the NIR band A and band B radiation, which accounts for 39% and 11% of the solar irradiance,[47] respectively, contribute to unwanted heat gain in the enclosed system. These two reflectors comprising indium tin oxide (ITO)/Ag/ITO as the NIR band B reflector and a total number of over 50 multilayer-polyethylene terephthalates[48] (PET) as the NIR band A reflector play pivotal roles in the management of solar heat. All combining structures of the four layers in the STRC outperformed other conventional O/M/O structures in lowering a cabin air temperature of 15.3 °C (Fig. S11). Investigation of the impact of varying solar irradiance on the surface temperature of the STRC revealed a direct correlation between increasing NIR reflectance and decreasing surface temperature (Fig. S3). To achieve a favorable outcome, carefully selected thicknesses of ITO, 60 nm, and Ag, 10 nm, were employed, which led to a high NIR reflectance and visible transmittance (Fig. S3).

Fabrication of STRC films

The samples used in this study are commercially available, including multilayer PET films (75 μm thick, PICASUS, Toray), conventional vehicle glass (2.1 mm thick, clear glass, Sanit-Gobain Korea), and PMMA (PR700, LX MMA). We implemented a novel manufacturing technique to tailor the entire spectrum, distinguishing our radiative cooling films from previous research.[10] Our process for creating the STRC films involved several steps. Initially, an ITO layers was deposited onto multilayer PET. This entailed deposition of a silver layer approximately 10 nm thick, followed by layers of ITO to optimize selective optical reflectance across the UV and NIR ranges. The layering sequence for this metamaterial structure was ITO/Ag/ITO. Subsequently, we applied a PMMA layer over the ITO layer to establish a comprehensive optical emitting surface. The hard coating with a thickness of 5 um was applied on the top of the STRC film. The STRC film's overall thickness measured approximately 190 μm. For Low-E performance comparison, we used a 3M Low-E film (85 μm thick, CC75, 3M)

Optical characterization and environmental durability of the STRC film

Solar transmittance and reflectance spectra (UV, visible, and NIR) spanning the 0.3–2.5 μm range were assessed using a UV-visible spectrophotometer (Agilent, Cary7000) equipped with an integrating sphere. Measurements of MIR absorptivity/emittance were conducted within the 2.5–18 μm range using a Fourier transform infrared spectrometer (Bruker, Vertex 70) featuring a gold integrating sphere (Mid-IR IntegratIR™, PIKE technologies) and mercuric cadmium telluride detector. The refractive indices of ITO, PMMA and SiO2 were measured using J.A. Woollam V-VASE and IR-VASE ellipsometers. An optical microscope with an upright Phoenix-MT was used to observe STRC, allowing photographs of water droplets on the STRC film surface to measure contact angles and determine surface wettability.

This study assessed the environmental durability of the material in relation to the proposed case demonstrations by conducting a series of durability tests. These tests included UV stability, mechanical tensile, material stability (DSC), Vickers hardness, and surface roughness evaluations. The UV stability test was performed continuously using an ATLAS Ci4400 system, with a cumulative exposure of 80 000 MJ. For the mechanical tensile test, conducted with an R&B INC UNITECH-T system, the test material was subjected to tension after 500 thermal cycles between −20 °C and 80 °C. Material stability for DSC was analyzed using a Polyma DSC214 with an aluminum crucible. The test involved a single cycle with temperature ramping from −40 °C to 90 °C, and heating and cooling rates were set at 10 °C min^{-1}. The Vickers hardness test was carried out using a Future tech FLV-AR series instrument. Finally, surface roughness was measured with a Keyence laser microscope.

Thermal measurements of the STRC film on the cabin

Experimental examinations of the transient thermal response of a STRC window were conducted on the roof of a Massachusetts Institute of Technology building in Cambridge, Massachusetts, U.S. Fig. 2b shows the experimental setup developed to measure the real-time temperature profiles. The setup

consisted of a 75-mm diameter cabin module and a surrounding thermal box. A transparent window of the chosen material and a black absorber were placed on the top and bottom of the cabin module, respectively. The vacant space encompassed the ambient air inside the cabin module. Three calibrated T-type thermocouples (TT-T-40-SLE-25, Omega) were placed in three different locations of the cabin module. The first thermocouple was laid between the absorber and a 24 mm thick vacuum insulation panel (U-Vacua, Panasonic) to measure the absorber temperature. The second thermocouple was placed in the middle of the cabin space for cabin temperature measurement. The thermocouple protruded from the cabin wall where the other end was taped. The third thermocouple was used to measure the window temperature and was taped to the bottom surface of the transparent window using optically clear adhesives (8146-2, 3M). The data from the three thermocouples were collected using a data logger (NI9213, CDAQ-9174, National Instrument). To suppress the conductive and convective heat exchange with the ambient air, we used thermally insulating polystyrene foam (FOAMULAR® 150, 30 cm × 30 cm × 7.5 cm) to fabricate a thermal box to uphold and insulate the cabin module. On the outer surfaces of the thermal box, silver-enhanced reflective aluminum sheets (Miro-20, Reflective Concepts) were applied to cover the exposed surfaces other than the cabin module to minimize the parasitic solar heating. The inner surface of the cabin module was covered with the aluminum foil tape to make it solar reflective.

The transient temperature profiles were recorded in real time for a 12-hour daytime period on four different days between October 10 and 14, 2023. The experiments began before sunrise at 5:00 am and ended at 5:00 pm. The weather station (HOBO U30 Station) was used to collect meteorological data, including ambient air temperature, solar irradiation, wind speed, and humidity. Measurements were conducted on two sunny days, one partial cloudy day, and one full cloudy day. Three identical experimental setups were fabricated for three transparent window materials: a STRC, a low-E film, and a conventional glass, to compare their cooling performances. The setups were placed 2 m above the ground to minimize the parasitic heat gained from the ground surface.

Vehicle outdoor thermal testing

We conducted 4-hour tests to establish the baseline vehicle performance. The average cabin air temperature difference between the vehicles was 0.29 °C, with a maximum difference of 0.57 °C, confirming comparable thermal characteristics. Baseline A/C cooling tests were also conducted, showing a cabin air temperature difference between vehicles $<2.5\%$ of the total test, thus ensuring a reliable evaluation of the technology without adjustments. Outdoor tests were conducted to alleviate STRC vehicle climate control loads. Each vehicle set comprised a control vehicle and a modified vehicle with STRC applied to the windows, enabling evaluation of each climate control load reduction strategy. Before testing, over 23 thermocouples were installed in each vehicle to measure the interior and exterior air and surface temperatures. The thermocouples were arranged in an eight-point pattern to measure the temperature of the cabin air at the headrests of the front and rear seats as well as the foot sections. To monitor system energy use, power sensors were also connected into each vehicle's high-voltage battery circuit. As part of the testing process, the cars were enclosed, undisturbed, and exposed to continuous sunlight exposure during a thermal soak phase that lasted from before morning until midday. Then, during the summer, the A/C activation phase in each car was started at the same time using the default maximum A/C settings—maximum blower speed, minimum air temperature threshold, and maximum air recirculation. During the winter, the heater activation phase in each car was started at the same time using the default maximum heating settings—maximum blower speed, maximum air temperature threshold, and full fresh mode.

Author contributions

M. J. L. conceived the idea and designed the present work. M. J. L., X. W., and Y. K. contributed to lab-scale experiments and data analyses. X. W., Y. K., and M. J. L. contributed to the thermal analysis and simulation. R. M. contributed to 1D steady-state and transient thermal modeling. B. J. L. contributed to optical simulations. T. H. K., J. H. S., H. J. L., and M. J. L. contributed to vehicle experiments and data analysis. W. S. K. contributed to vehicle simulation. M. J. L. authored the manuscript, and all reviewed the manuscript. S. H. K supervised and reviewed the present work. G. C contributed to manuscript writing, data interpretation and supervised research at MIT.

Conflicts of interest

A KR patent (application no. 1020230179087) related to this work has been filed. M. J. L., T. H. K., W. S. K., J. H. S., H. J. L., and S. H. K. are inventors of this filed patent.

Data availability

Data supporting this article are included in the supplementary information (SI). The supplementary information includes additional optical simulations, experimental setups, extended vehicle test data, and detailed thermal modeling methods supporting the main findings. See DOI: https://doi.org/10.1039/d5ee06609c.

Acknowledgements

We thank Byung Hong Lee for his helpful discussion on STRC material studies and Hyun Gu Lee for visualization of the vehicle figure. This work was supported by the National Research Foundation of Korea (grant no. RS-2025-11092968 and RS-2025-02223634) and the Hyundai Motor Company (grant no. R-220505.0001 and R-220505.0004).

References

1 G. J. Marshall, *et al.*, Thermal Management of Vehicle Cabins, External Surfaces, and Onboard Electronics: An Overview, *Engineering*, 2019, **5**, 954–969, DOI: 10.1016/j.eng.2019.02.009.
2 E. Alayed, D. Bensaid, R. O'Hegarty and O. Kinnane, Thermal mass impact on energy consumption for buildings in hot climates: A novel finite element modelling study comparing building constructions for arid climates in Saudi Arabia, *Energy Build.*, 2022, **271**, 112324, DOI: 10.1016/j.enbuild.2022.112324.
3 S. Somasundaram, S. R. Thangavelu and A. Chong, Improving building efficiency using low-e coating based retrofit double glazing with solar films, *Appl. Therm. Eng.*, 2020, **171**, 115064, DOI: 10.1016/j.applthermaleng.2020.115064.
4 N. Abundiz-Cisneros, *et al.*, Novel Low-E filter for architectural glass pane, *Energy Build.*, 2020, **206**, 109558, DOI: 10.1016/j.enbuild.2019.109558.
5 B. P. Jelle, S. E. Kalnæs and T. Gao, Low-emissivity materials for building applications: A state-of-the-art review and future research perspectives, *Energy Build.*, 2015, **96**, 329–356, DOI: 10.1016/j.enbuild.2015.03.024.
6 A. Grundstein, V. Meentemeyer and J. Dowd, Maximum vehicle cabin temperatures under different meteorological conditions, *Int. J. Biometeorol.*, 2009, **53**, 255–261, DOI: 10.1007/s00484-009-0211-x.
7 M. Lee, *et al.*, Photonic structures in radiative cooling, *Light: Sci. Appl.*, 2023, **12**, 134, DOI: 10.1038/s41377-023-01119-0.
8 E. M. Zhiyu Hu, *Infrared Radiative Cooling and Its Applications*, Springer, Singapore, 2022.
9 A. P. Raman, M. A. Anoma, L. Zhu, E. Rephaeli and S. Fan, Passive radiative cooling below ambient air temperature under direct sunlight, *Nature*, 2014, **515**, 540–544, DOI: 10.1038/nature13883.
10 Y. Zhai, *et al.*, Scalable-manufactured randomized glass-polymer hybrid metamaterial for daytime radiative cooling, *Science*, 2017, **355**(6329), 1062–1066, DOI: 10.1126/science.aai7899.
11 X. Yin, R. Yang, G. Tan and S. Fan, Terrestrial radiative cooling Using the cold universe as a renewable and sustainable energy source, *Science*, 2020, **370**, 786–791.
12 J. Mandal, *et al.*, Hierarchically porous polymer coatings for highly efficient passive daytime radiative cooling, *Science*, 2018, **362**(6412), 315–319, DOI: 10.1126/science.aat951.
13 D. Li, *et al.*, Scalable and hierarchically designed polymer film as a selective thermal emitter for high-performance all-day radiative cooling, *Nat. Nanotechnol.*, 2021, **16**, 153–158, DOI: 10.1038/s41565-020-00800-4.
14 B. Bhatia, *et al.*, Passive directional sub-ambient daytime radiative cooling, *Nat. Commun.*, 2018, **9**, 5001, DOI: 10.1038/s41467-018-07293-9.
15 W. Li, Y. Shi, Z. Chen and S. Fan, Photonic thermal management of coloured objects, *Nat. Commun.*, 2018, **9**, 4240, DOI: 10.1038/s41467-018-06535-0.
16 X. Zhao, *et al.*, A solution-processed radiative cooling glass, *Science*, 2023, **382**(6671), 684–691, DOI: 10.1126/science.adi2224.
17 D. Zhao, *et al.*, Subambient Cooling of Water: Toward Real-World Applications of Daytime Radiative Cooling, *Joule*, 2019, **3**, 111–123, DOI: 10.1016/j.joule.2018.10.006.
18 E. A. Goldstein, A. P. Raman and S. Fan, Sub-ambient non-evaporative fluid cooling with the sky, *Nat. Energy*, 2017, **2**, 17143, DOI: 10.1038/nenergy.2017.143.
19 S. Y. Heo, *et al.*, A Janus emitter for passive heat release from enclosures, *Sci. Adv.*, 2020, **6**(36), eabb1906, DOI: 10.1126/sciadv.abb1906.
20 K. Lin, *et al.*, Hierarchically structured passive radiative cooling ceramic with high solar reflectivity, *Science*, 2023, **382**(6671), 691–697, DOI: 10.1126/science.adi4725.
21 T. Li, *et al.*, A radiative cooling structural material, *Science*, 2019, **364**(6442), 760–763, DOI: 10.1126/science.aau9101.
22 W. Zhu, *et al.*, Large-scale industry-compatible sub-ambient radiative cooling pulp, *Cell Rep. Phys. Sci.*, 2022, **3**(11), 101125, DOI: 10.1016/j.xcrp.2022.101125.
23 C. Ibekwe, *et al.*, Synthesis, Optical Performance Characterization, and Durability of Electrospun PTFE-PEO Materials for Space Applications, *ACS Appl. Mater. Interfaces*, 2024, **16**, 32587–32598, DOI: 10.1021/acsami.4c02463.
24 Y. Lv, A. Huang, J. Yang, J. Xu and R. Yang, Improving cabin thermal environment of parked vehicles under direct sunlight using a daytime radiative cooling cover, *Appl. Therm. Eng.*, 2021, **190**, 116776, DOI: 10.1016/j.applthermaleng.2021.116776.
25 Z. Zhou, X. Wang, Y. Ma, B. Hu and J. Zhou, Transparent Polymer Coatings for Energy-Efficient Daytime Window Cooling, *Cell Rep. Phys. Sci.*, 2020, **1**(11), 100231.
26 M. Kim, *et al.*, Visibly Transparent Radiative Cooler under Direct Sunlight, *Adv. Opt. Mater.*, 2021, **9**, 2002226, DOI: 10.1002/adom.202002226.
27 M.-Q. Lei, *et al.*, Transparent radiative cooling films containing poly(methylmethacrylate), silica, and silver, *Opt. Mater.*, 2021, **122**(Part B), 111651, DOI: 10.1016/j.optmat.2021.111651.
28 Y. Jin, Y. Jeong and K. Yu, Infrared-Reflective Transparent Hyperbolic Metamaterials for Use in Radiative Cooling Windows, *Adv. Funct. Mater.*, 2022, **33**, 2207940, DOI: 10.1002/adfm.202207940.
29 S. Kim, *et al.*, High-Performance Transparent Radiative Cooler Designed by Quantum Computing, *ACS Energy Lett.*, 2022, **7**, 4134–4141, DOI: 10.1021/acsenergylett.2c01969.
30 Y. Zhu, *et al.*, Color-preserving passive radiative cooling for an actively temperature-regulated enclosure, *Light: Sci. Appl.*, 2022, **11**, 122, DOI: 10.1038/s41377-022-00810-y.
31 Y. Li, *et al.*, Janus Interface Engineering Boosting Visibly Transparent Radiative Cooling for Energy Saving, *ACS Appl. Mater. Interfaces*, 2023, **15**, 4122–4131, DOI: 10.1021/acsami.2c20462.
32 ed. Katipamula, N. F. W. W. K. A. S. U.S. Department of Energy) (Pacific Northwest National Laboratory, Washington, 2015).
33 H. H. Al-Kayiem, M. F. B. M. Sidik and Y. R. A. L. Munusammy, Study on the Thermal Accumulation and Distribution Inside a Parked Car Cabin, *Am. J. Appl. Sci.*, 2010, **7**, 784, DOI: 10.3844/ajassp.2010.784.789.

34 American Society of Heating, R., and AirConditioning Engineers. *Standard 55-2013 User's Manual: ANSI/ASHRAE Standard 55-2013, Thermal Environmental Conditions for Human Occupancy*. (2016).
35 K. W. Lee, *et al.*, Visibly Clear Radiative Cooling Metamaterials for Enhanced Thermal Management in Solar Cells and Windows, *Adv. Funct. Mater.*, 2021, **32**, 2105882.
36 S. Dang, X. Wang and H. Ye, An Ultrathin Transparent Radiative Cooling Photonic Structure with a High NIR Reflection, *Adv. Mater. Interfaces*, 2022, **9**, 2201050, DOI: 10.1002/admi.202201050.
37 ed. Agency, U. S. E. P., Office of Transportation and Air Quality) (Office of Transportation and Air Quality, MI, 2023).
38 C. Choi, *et al.*, Light-Wavelength-Selective Transparent ITO/Ag/ITO/Ag/ITO Structure for Functional Energy Applications, *Solar RRL*, 2023, **8**, 2300936, DOI: 10.1002/solr.202300936.
39 C. Guillén and J. Herrero, SnO_x/Ag/SnO_x heat-reflector coatings prepared by DC sputtering, *SN Appl. Sci.*, 2020, **2**, 1717, DOI: 10.1007/s42452-020-03508-1.
40 S. Wang, *et al.*, Scalable thermochromic smart windows with passive radiative cooling regulation, *Science*, 2021, **374**(6574), 1501–1504, DOI: 10.1126/science.abg0291.
41 K. Tang, *et al.*, Temperature-adaptive radiative coating for all-season household thermal regulation, *Science*, 2021, **374**(6574), 1504–1509, DOI: 10.1126/science.abf7136.
42 X. Wang and S. Narayan, Thermal radiative switching interface for energy-efficient temperature control, *Renewable Energy*, 2022, **197**, 574–582, DOI: 10.1016/j.renene.2022.07.143.
43 X. Wang and S. Narayan, Thermochromic Materials for Smart Windows: A State-of-Art Review, *Front. Energy Res.*, 2021, **9**, 800382, DOI: 10.3389/fenrg.2021.800382.
44 V. Soulios, R. C. G. M. Loonen, V. Metavitsiadis and J. L. M. Hensen, Computational performance analysis of overheating mitigation measures in parked vehicles, *Appl. Energy*, 2018, **231**, 635–644, DOI: 10.1016/j.apenergy.2018.09.149.
45 X. Yin, R. Yang, G. Tan and S. Fan, Terrestrial radiative cooling: Using the cold universe as a renewable and sustainable energy source, *Science*, 2020, **370**, 786–791, DOI: 10.1126/science.abb0971.
46 S. Fan and W. Li, Photonics and thermodynamics concepts in radiative cooling, *Nat. Photonics*, 2022, **16**, 182–190, DOI: 10.1038/s41566-021-00921-9.
47 J. Mandal, Y. Yang, N. Yu and A. P. Raman, Paints as a Scalable and Effective Radiative Cooling Technology for Buildings, *Joule*, 2020, **4**, 1350–1356, DOI: 10.1016/j.joule.2020.04.010.
48 Y. Matsuo, T. Uto, S. Osada and W. Goda, WO2013137288 – Multi-layer laminated film, 2013.